International Journal of Thermodynamics (IJoT)
ISSN 1301-9724 / e-ISSN 2146-1511
https://dergipark.org.tr/en/pub/ijot

Vol. 25 (No. 2), pp. 001-006, 2022
doi: 10.5541/ijot.988667
Published online: June 1, 2022

Thermodynamic Bases for Obtaining Crystalline Perfect Silicon from Tin-silicon Solution

Alijon Razzokov Shonazarovich[1*], Khushnudbek Eshchanov Odilbekovich[2]

[1]Department of Physics, Urgench State University, Urgench, Uzbekistan
[2]Department of Chemistry, Urgench State University, Urgench, Uzbekistan
E-mail: [1]razzokov.a@bk.ru

Received 30 August 2021, Revised 8 January 2022, Accepted 22 February 2022

Abstract

Silicon epitaxial layers were grown on a silicon (Si<111>) substrate in the range of 1323÷1073 K with initial crystallization temperatures from the silicon-tin (Si-Sn) solution. To determine the forces acting between the silicon nanoclusters in solution and the tin (Sn) particles and the silicon (Si) surface, the dielectric constant values of silicon, tin at selected temperatures were found experimentally. Given the Gibbs energy of the system to obtain the perfect epitaxial layers and structures of the crystal, optimal technological growth conditions are given.

Keywords: *Epitaxy, nanocluster, crystallization, solution-melt, dislocation, dielectric constant.*

1. Introduction

Semiconductor materials CdTe, CdS, GaAs, GaP, GaSb, GaN, InSb, InP, InAs, ZnSe, ZnS and solid solutions obtained on their basis $Al_xGa_{1-x}As$, $Al_xGa_{1-x}P$, $GaAs_{1-x}P_x$, $Ga_xIn_{1-x}As$, although they have high photoelectric parameters and are used as active elements in the development of optoelectronic devices, however, the synthesis of high-quality crystals of binary compounds is a technologically difficult task, therefore they are expensive materials. The manufacture of massive elements based on binary compounds is impractical. However, the possibility of obtaining a relatively low temperature of epitaxial silicon films from a solution-melt on relatively cheap silicon substrates makes them widely used materials. Therefore, the elucidation of the physicochemical features, i.e. The thermodynamic foundations of growing epitaxial Si films from a solution-melt remain one of the urgent problems of modern semiconductor physics. Using the literary known parameters, as well as conducting an experimental study to determine some constants and quantities, it is shown that crystalline perfect silicon grows under optimal conditions. It has been established that the optimal technological growth mode with the lowest energy costs.

The authors of [1, 2] attempted to obtain structurally perfect silicon epitaxial layers from a tin solution-melt. To accomplish this, they investigated the technological growth modes, electrical, photoelectric properties of epitaxial silicon layers.

However, those modes of technological growth, which are associated with the physical and chemical properties of the grown solution-melt of such a system, have not been thoroughly researched too far.

2. Theoretical Part

In a metastable system, crystallization occurs in two stages: a forced stage of nucleation—the formation of an interface, and the second spontaneous stage—growth on a seed. As a result, at the growth stage, the following main processes and related stages can be differentiated: delivery of a substance to a growing crystal (transport processes in the environment) and its attachment (kinetic phenomena on the surface).

During the forced growth of epitaxial layers at the crystal-liquid boundary, the isobaric-isothermal potential of the system ($\Delta G_{cr}>0$) increases. The free energy varies depending on the surface size and its surface energy σ.

A very important factor in the binding growth of silicon is the solvent and the substrate material, which has a specific orientation (In our study, the solvent was tin or gallium, and the substrate was oriented silicon <111>).

Despite $\Delta G_{cr}>0$, epitaxial silicon layers grow on the substrate due to surface energy in diffusion-kinetic or mixed mode. It should also be noted that the fact that the size of the crystal-forming nanoclusters in the system is in a critical state ($\Delta G_{cr}>0$) causes the crystallization process to begin. When nanoclusters of critical size are placed on the substrate, a $\Delta G_{cr}<0$ condition occurs when new 2D-sized primary centres larger than the critical size begin to appear (Figure 1). This condition is energetically preferred for the growth of epitaxial layers on the substrate surface.

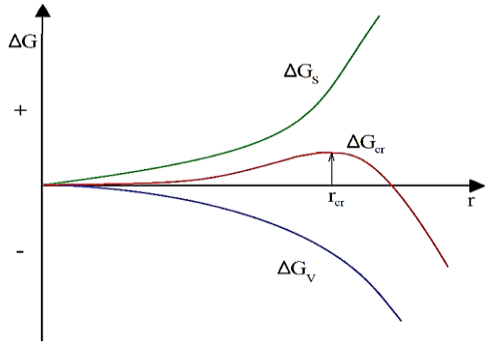

Figure 1. Volumetric Gibbs energy-G_v, surface Gibbs energy-ΔG_s and total Gibbs energy representing cluster formation-ΔG_{cr}, dependence on cluster radius.

*Corresponding Author

When a substrate isn't available (solid surface), self-formation of nanoparticles occurs during cooling, however, this interferes with getting a single crystal from a homogeneous solution melt. As a result, a silicon substrate is used, which shares the same atomic radius of the crystallized film and substrate, as well as the coefficient of thermal expansion of the materials. All of these processes, however, are always specified by technological parameters, such as temperature, cooling rate, solvent type, and so on. Therefore, we will provide novel theoretical calculations for obtaining a film of a silicon single crystal on a silicon substrate with the lowest energy consumption and dislocation density. This is very important in production. For the ideal case of a silicon system dissolved in a tin liquid, the mixing Gibbs energy is as follows [3, 4, 5].

$$\Delta G_{mix} = RT(X_1 \ln X_1 + X_2 \ln X_2) \quad (1)$$

In real systems, the activity must be used instead of the moles of the solution's components. In this example, in contrast to formula (1), the Gibbs energy of the interference is given in the form below [3, 4].

$$\Delta G_{mix} = RT(X_1 \ln a_1 + X_2 \ln a_2) \quad (2)$$

The following expression can be used to determine the activity in formula [4, 5, 6]:

$$a = \gamma \cdot X \quad (3)$$

Here, X-mole fraction, γ -activity coefficient.

On the other hand, the determination of the magnitude of the expression γ is based on experimental results. The formula (4) was used to calculate the activity coefficient for the silicon component.

$$\lg \gamma_{Si} = \frac{a' - b' T_{(s)(Si)}}{R T_{(s)(Si)}} (1 - X_{Sn})^2 \quad (4)$$

The values of the constants *a'* and *b'* in the formula are determined experimentally. For the Si–Sn system, *a'*=31162 and *b'*=4.0289 are found [7, 8, 9].

The detected activities of silicon and tin in the Si-Sn system (*a*) are given in the following table (Table 1).

Table 1. Silicon and tin activity values.

№	T	*a*(Sn)	*a*(Si)
1	1373 K	0.8785675	0.5857100
2	1323 K	0.914285	0.4285700
3	1273 K	0.942855	0.3047617
4	1223 K	0.961000	0.2071425
5	1173 K	0.975285	0.1571400
6	1123 K	0.989570	0.1328555
7	1073 K	0.999000	0.0142850

Using the data in the table, the interference of the Si-Sn system was determined by the Gibbs energy (Figure 2).

The graph depicts how the Gibbs energy values of the system's mixing drop as the temperature rises. This shows that the system's silicon solubility in the tin solution is increasing.

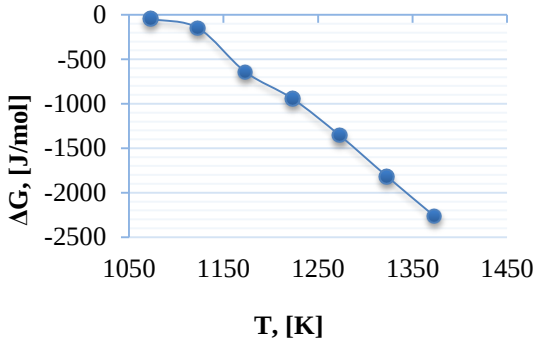

Figure 2. Gibbs temperature dependence graph of system interference

Silicon crystals occur during the cooling of the Si-Sn system. Formula (1) is used to calculate the total Gibbs energy for the crystallization process in the system (formula (5)) [3, 10].

$$\Delta G_{system} = \Delta G_{cr} + \Delta G_{mix.then} - \Delta G_{mix.first} \quad (5)$$

Silicon nanoclusters were considered to be formed during the cooling of the system. The formation of silicon nanoclusters can be seen as the beginning of the primary crystallization process in the system [11, 12, 13, 14, 15]. The Gibbs (ΔG_{cr}) energy for the formation of silicon nanocrystals in a liquid tin medium was calculated using the following formulas [16]. The results of the calculation are shown in Figure 3.

$$r_c = \frac{2\sigma_{s-l} V_m}{\mu_1 - \mu_2} = \frac{2\sigma_{s-l} \cdot V_m \cdot T_l}{L \cdot \Delta T} \quad (6)$$

$$\mu_1 - \mu_2 = \Delta G_v = L \frac{\Delta T}{T_l} \quad (7)$$

$$\Delta G_{cr} = \frac{16\pi\sigma_{s-l}{}^3 V_m{}^2}{3(\Delta G_v)^2} \quad (8)$$

Here, μ_1 and μ_2 -chemical potential of liquid and solid silicon, V_m-molar volume of silicon, L -the heat of fusion of silicon, σ_{s-l} -solid-liquid interface surface tension of silicon.

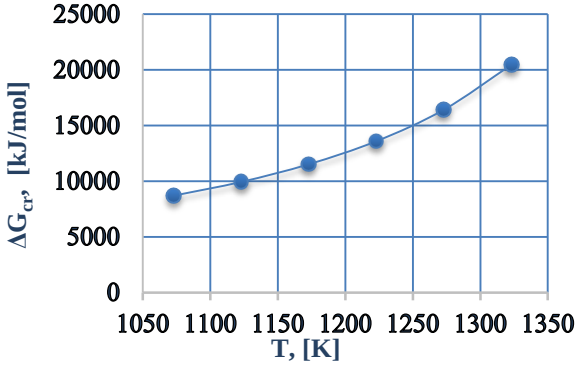

Figure 3. Formation of silicon nanocrystals Gibbs temperature dependence graph.

The silicon nanoclusters generated in the system settle on the surface of the silicon embedded in the system, forming a macro-sized single crystal. For each temperature,

the total Gibbs energy of the system was calculated using the formula (5) (Figure 4).

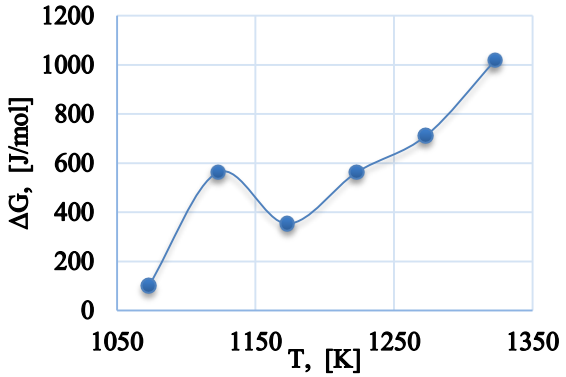

Figure 4. Gibbs energy in the formation of silicon crystals in the system temperature dependence graph.

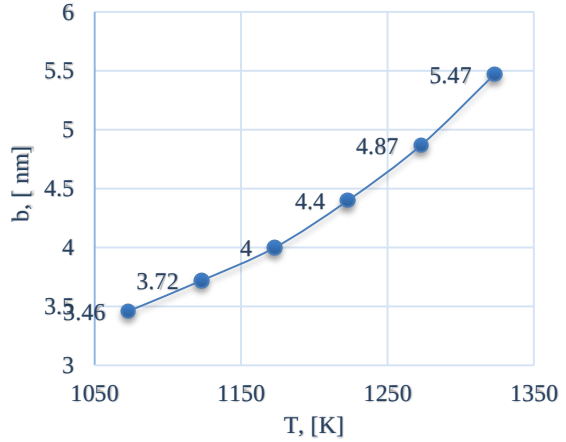

Figure 5. Temperature dependence of different sizes of dislocation centers relative to the growing surface.

Examination of the formation of silicon crystals at different temperatures revealed that the different sizes of the dislocation centres on the crystal-forming surface (base) decreased with decreasing temperature (Figure 5) [16]. However, as can be seen from the graph in Figure 4, during crystallization at 1173 K, the Gibbs energy of the system has a specific decrease, while the Gibbs energy of the system has increased again at 1123 K. This reduces the probability of the formation of silicon crystals from 1173 K to 1123 K. Even at temperatures below 1123 K, a decrease in the Gibbs energy of the system is observed during crystallization. However, the amount of silicon in the Si-Sn system remains very low at temperatures below 1123 K (0.001 mole fraction).

3. Method and Materials

Chemically pure samples of tin and silicon were used for the experiment. Silicon plate in the <111> direction was used as the substrate.

The experiment was carried out in an EPOS-type device (Pd-15T purifier) and in a hydrogen atmosphere at a temperature of 333-1323 K. The LVT 9/11-Nabertherm heater was used for heat transfer. A 4-Channel Type-K thermometer was used to check the temperature.

4. Experimental Part

Epitaxial layers of a silicon single crystal were grown from a tin and gallium solution-melt on single-crystal Si substrates with (<111>) p and n-type conductive liquid-phase epitaxy according to the technology described in [17]. The substrates were 20 mm in diameter and ~400 μm in thickness.

The composition of the solution-melt, consisting of silicon and tin, as well as silicon and tin, was determined from the phase diagram of the Sn–Si and Ga–Si binary alloy. The solubility of silicon in the tin was investigated at temperatures ranging from 1073 to 1373 K in order to create a liquid solution melt. Epitaxial silicon films were grown at temperatures of the onset (T_{oc}) and end of crystallization (T_{ec}), respectively, in the range 1323÷1073 K. The samples were grown at different values of the technological parameters of liquid epitaxy. A high-quality silicon single crystal with a dislocation density of $5\cdot10^4\div9\cdot10^3$ cm^{-2} was obtained.

The interaction forces of the particles in the system have been studied in the nanoscale explanation of the growth of low-defect and dislocated silicon epitaxial layers from the Si-Sn liquid solution to the Si surface. Here, silicon nanoclusters interact with the growing surface to participate in the formation of silicon single crystals on the surface [16]. The forces of interaction of the formed silicon nanoclusters with the solvent tin particles in the system, as well as with the particles on the surface of the growing silicon substrate (Lennard-Jones forces) were calculated [18, 19, 20].

$$U_{L-J} = \frac{A}{r_{AB}^{12}} - \frac{B}{r_{AB}^{6}} \tag{9}$$

$$B = \frac{3\cdot\alpha_{Si}\cdot\alpha_{Sn}\cdot I_{Si}\cdot I_{Sn}}{2\cdot(4\pi\varepsilon_0)^2\cdot(I_{Si}+I_{Sn})} \tag{10}$$

$$\alpha = 4\pi\varepsilon_0 R_p^{\,3}\frac{\varepsilon-1}{\varepsilon+2} \tag{11}$$

$$\sigma = \frac{r}{2^{1/6}} \tag{12}$$

$$A = B\cdot\sigma^6 \tag{13}$$

Where σ is the distance at which the intermolecular potential between the two particles is zero. A and B are constants, which depend on the type and particle composition. r- is the contact distance of the particles, I-ionization potential of the particle, α-polarity, R_p-particle radius, ε-dielectric constant, ε_0=8,85·10^{-12} F/m.

To determine the Lennard-Jones forces from formula (7), it is necessary to determine the quantities A and B. Formula (8) is used to determine the magnitude of B [21, 22]. The quantities α_{Si} and α_{Sn} in formula (8) are the polarity of silicon and tin in solution. As the crystallization process in the system took place at different high temperatures, it became necessary to determine the dielectric constant of the particles to know the polarity values at the same temperatures (polarity was determined using the formula (11)).

Since there is almost no data on the dielectric constant of silicon and tin in the scientific literature, we determined the parameters experimentally (Figures 6-7) [23, 24].

The dielectric constant of silicon was determined in a parallel-plate capacitor, while that of a tin metal was

determined in a hemispherical capacitor chain. The detection process was carried out in a hydrogen atmosphere.

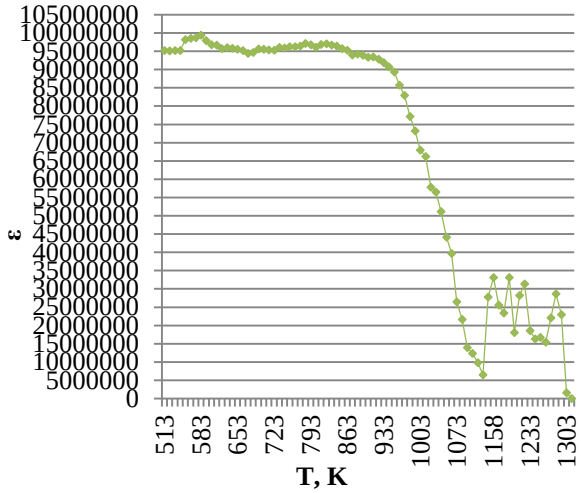

Figure 6. Dielectric constant values of tin metal at different temperatures.

According to the scientific literature [25, 26], the dielectric constant of metals is very high at room temperature, as shown in Figure 6. Experiments have shown that the dielectric constant of tin averages $9.6 \cdot 10^7$ from 513 K to 883 K. There was a decrease in dielectric constant from 883 K to 1133 K, an increase and decrease from 1133 K to 1283 K, and a sharp decrease from 1283 K to 1323 K.

Based on the experimental results, it can be said that the change in the metallic properties of tin is observed when the temperature exceeds 883 K. It can be assumed that the structure (chemical bonds, shape) in the liquid medium is unstable when the values of dielectric refractive index in the range of 1133÷1323 K are not regulated.

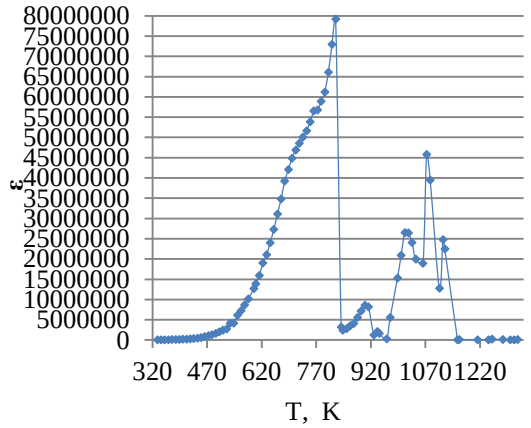

Figure 7. Dielectric constant values of silicon at different temperatures.

In the experiment, we determined the values of dielectric constant of silicon at temperatures of 333÷1323 K. It can be seen that the values of dielectric constant increase in the temperature range of 333÷823 K, and sharply decrease from 823 K to 843 K. It was observed that the dielectric constant values from 843 K to 1158 K were in the form of irregular increase and decrease. Differences in the dielectric constant of silicon decreased from 1158 K to 1323 K (Figure 7).

Based on the dielectric constant values determined experimentally at the selected appropriate crystallization temperatures of silicon and tin, the Lennard-Jones interaction forces of the tin solvent particles and the growing surface of silicon nanoclusters were calculated using formulas (9)-(13) (Table 2, Figure 8).

Table 2. Temperature dependence of Lennard-Jones force values between silicon surface and silicon nanoclusters.

T_{cr}	Cluster radius	$B \cdot 10^{-74}$	$A \cdot 10^{-127}$	$U_{L\text{-}J} \cdot 10^{-22}$ J (Si_{nano}-$Si_{surface}$)
1323 K	2.60 nm	3.7517	5.6185	-901.857
1273 K	2.33 nm	2.700	3.155	-670.132
1223 K	2.10 nm	1.9769	1.6459	-557.980
1173 K	1.90 nm	1.4638	0.769	-536.382
1123 K	1.77 nm	1.1836	0.5677	-413.300
1073 K	1.65 nm	0.959	0.3986	-334.544
1023 K	1.54 nm	0.779	0.2758	-275.000

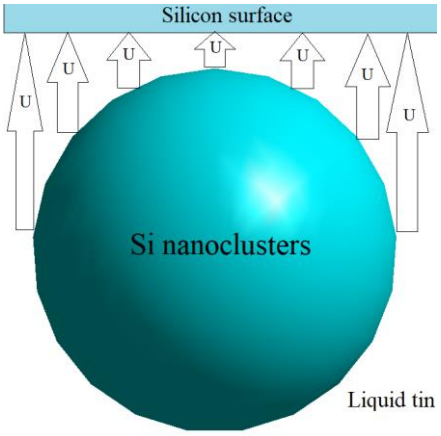

Figure 8. Scheme of the interaction between the substrate surface and the silicon nanocluster in the liquid tin medium.

In a silicon-tin solution, the strengths of silicon nanoclusters forming silicon single crystals on the silicon surface increase with increasing temperature. Consequently, the probability of a covalent bond between the surface and the silicon nanocluster increases due to an increase in the Lennard-Jones forces. This process leads to the formation of a single crystal on the surface on which it grows.

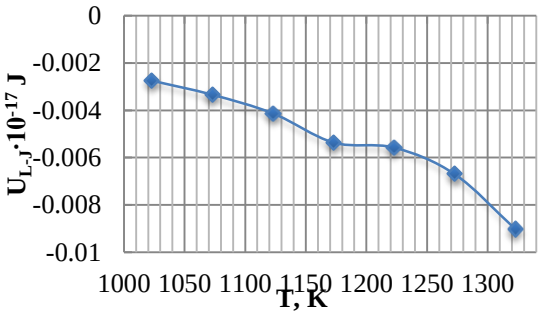

Figure 9. Lennard-Jones forces between silicon nanoclusters, which form silicon single crystals, and crystallization at different temperatures.

In a silicon-tin solution, the interaction potential between the silicon nanocluster and tin particles also increases in the arc direction with decreasing temperature (Table 3).

Table 3. Temperature dependence of Lennard-Jones force values between tin particles and silicon nanoclusters.

T_{cr}	Cluster radius	$B \cdot 10^{-74}$	$A \cdot 10^{-131}$	$U_{L\text{-}J} \cdot 10^{-22}$ J (Si_{nano}-Sn_m)
1323 K	2.60 nm	4.4697	3.2584	-39635570
1273 K	2.33 nm	3.2165	2.3448	-23666760
1223 K	2.10 nm	2.3557	1.7179	-14564514
1173 K	1.90 nm	1.9383	1.4130	-10151320
1123 K	1.77 nm	1.4105	1.0280	- 6578138
1073 K	1.65 nm	1.1440	0.8340	-4630000
1023 K	1.54 nm	0.9300	0.6779	-3482447.8

It was found that the interaction potential values of tin particles with silicon nanoclusters change from a temperature of 1323 K to a temperature of 1073 K on a curved line, and at temperatures below 1073 K on a straight line (Figure 10-11).

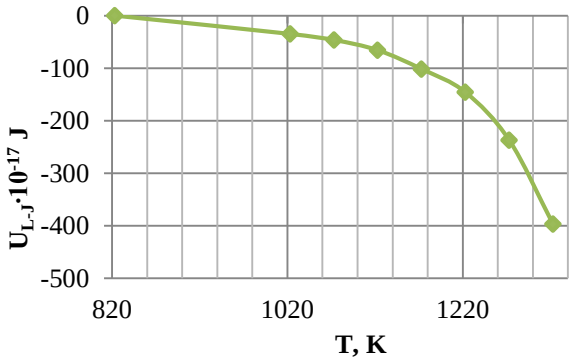

Figure 10. Lennard-Jones interaction forces between silicon nanoclusters and tin particles that form silicon single crystals during crystallization at different temperatures.

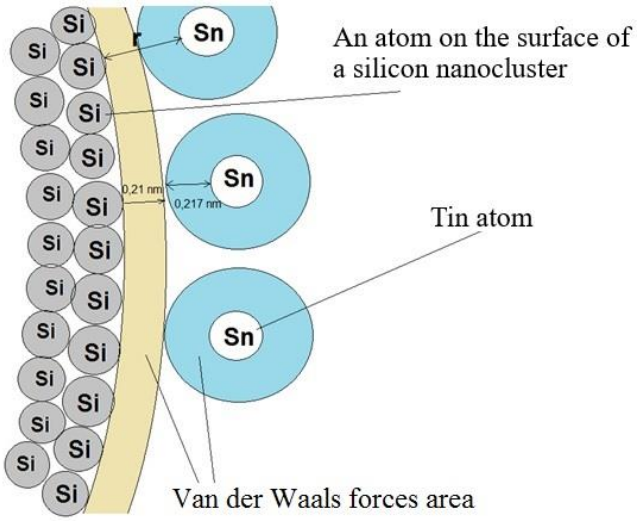

Figure 11. Scheme of the interaction of silicon nanoclusters and tin particles.

From experiments and theoretically determined indicators, it can be concluded that as the initial temperatures of single crystal growth decrease, the Si-Si impact forces increase. However, at the film-base boundary, the dislocation density increases exponentially when the temperature is high at the beginning of the growth process. This can be explained by the relatively large size of the initial nanocluster in the formation of the single crystal (Table 2). Therefore, the conditions are chosen to grow crystalline perfect epitaxial layers with relatively low dislocation density of the required thickness in accordance with the Si base orientation. This is based on the above experimental and theoretical measurement calculations performed by us.

5. Conclusion

The energy and technological conditions for the growth of silicon epitaxial layers from the liquid Si-Sn system to the silicon surface to crystalline perfect, ie low dislocation, were investigated. The optimal energy conditions for the growth of silicon single crystals were calculated theoretically, the Gibbs energy of the system, the size of the silicon nanocluster forming the single crystal, the size of the dislocation centres relative to the surface were calculated, and a temperature of 1173 K was chosen for growing the silicon single crystal from Si-Sn. The experiment was carried out based on these theoretical results, and a high-quality silicon single crystal with a dislocation density of $5 \cdot 10^4 \div 9 \cdot 10^3$ cm^{-2} was obtained.

Nomenclature

a	*Activity*
γ	*Activity coefficient*
ΔG	*Changes in Gibbs energy, J/mol*
R	*Universal gas constant, 8,314 $J \cdot K^{-1} \cdot mol^{-1}$*
T	*Temperature, K*
X	*Mole fraction*
r_c	*Critical radius of the particle, m*
$\sigma_{s\text{-}l}$	*solid-liquid surface tension, J/m^2*
V_m	*Molar volume, m^3*
μ	*Chemical potential, J/mol*
L	*Heat of fusion, J/mol*
b	*Size of dislocation centers, nm*
$U_{L\text{-}J}$	*Lennard-Jones forces, J*
r	*Distance between particles, m*
σ	*Distance at which the intermolecular potential between the two particles is zero, m*
ε	*Dielectric constant*
ε_0	*Electric constant, $8{,}85 \cdot 10^{-12}$ F/m*
α	*Polarity*
I	*Ionization potential, J*
R_p	*The radius of the polar particle, m*

References:

[1] A. Nikiforov, V. Timofeev, V. Mashanov, T. Gavrilova and D. Gulyaev, "Elastically stressed pseudomorphic SiSn island array formation with a pedestal on the Si(100) substrate using Sn as a growth catalyst", *Journal of Crystal Growth*, vol. 518, pp. 103-107, 2019. Available: https://doi.org/10.1016/j.jcrysgro.2019.04.021.

[2] K. Fujiwara, "Crystal Growth Behaviors of Silicon during Melt Growth Processes", *International Journal of Photoenergy*, pp. 1-16, 2012. Available: https://doi.org/10.1155/2012/169829.

[3] Gaskell, D.R., & Laughlin, D.E. *Introduction to the Thermodynamics of Materials*, 6th Ed. CRC Press, 2017. Available: https://doi.org/10.1201/9781315119038.

[4] Arthur D. Pelton. *Phase Diagrams and Thermodynamic Modeling of Solutions*, Elsevier. 2019. Available: https://doi.org/10.1016/C2013-0-19504-9.

[5] Kaufman Myron, *Principles of Thermodynamics*, CRC Press, p. 213, 2002. ISBN 978-0-8247-0692-0

[6] Guggenheim, E.A. "The Conceptions of Electrical Potential Difference between Two Phases and the Individual Activities of Ions". *Journal Physcal Chemistry*, vol. 33, (6), pp. 842–849, 1929. Available: https://doi.org/10.1021/j150300a003.

[7] J. Safarian, L. Kolbeinsen, and M. Tangstad, "Thermodynamic activities in silicon binary melts," *Journal of Materials Science*, vol. 47, no. 14, pp. 5561–5580, 2012. Available: https://doi.org/10.1007/s10853-012-6449-4.

[8] Michael J. Moran, Howard N. Shapiro, Daisie D. Boettner, Margaret B. Bailey. *Fundamentals of Engineering Thermodynamics*, 3rd Ed. Michael J., Wiley –Interscience, 2010. ISBN 0-471-07681-3

[9] L. S. Darken, "Application of the Gibbs-duhem equation to ternary and multicomponent systems," *Journal of the American Chemical Society*, vol. 72, no. 7, pp. 2909–2914, 1950. Available: https://doi.org/10.1021/ja01163a030.

[10] S. Uda, X. Huang, S.Koh. *Journal of Crystal Growth*, vol. 281, pp. 481–491, 2005.

[11] P. Rudolph, in: *Crystal growth Technology*, H.J. Scheel and T. fukuda (eds.) Wiley –Interscience, 2003.

[12] E. D. Shukin, A. V. Persov, E.A. Ameline. *Colloid chemistry*, -M.: Higher. sch., 2004.

[13] Ivan Markov. *Crystal Growth For Beginners: Fundamentals of Nucleation, Crystal Growth And Epitaxy*, 3th Ed. Singapore: World Scientific, 2016. Available: https://doi.org/10.1142/10127.

[14] Burton, W. K.; Cabrera, N. *"Crystal growth and surface structure. Part I"*. Discussions of the Faraday Society, 1949. Available: https://doi.org/10.1039/DF9490500033.

[15] Burton, W.K.; Cabrera, N. *"Crystal growth and surface structure. Part II"*. Discussions of the Faraday Society, 1949. Available: https://doi.org/10.1039/DF9490500040.

[16] Razzokov, A.Sh., Khakimov, N.Z., Davletov, I.Y., Eshchanov, Kh.O. and Matnazarov, A.R. "Obtaining a structurally perfect semiconductor solid solution $Si_{1-x}Ge_x$ with electrophysical and photoelectric properties," *Scientific-technical journal*, vol. 24, iss. 5, pp. 11, 2020. Available: https://uzjournals.edu.uz/ferpi/vol24/iss5/11.

[17] Saidov, A.S., Razzokov, A. Sh. "Obtaining and morphological studies of epitaxial layers of the $Si_{1-x}Ge_x$ solid solution", *Siberian Physical Journal*, vol. 15, no. 2, pp. 84–91, 2020. Available: https://doi.org/10.25205/2541-9447-2020-15-2-84-91.

[18] Lennard-Jones, J.E. "Cohesion". *Proceedings of the Physical Society*, vol. 43 no. 5, pp. 461–482, 1931. Available: https://doi.org/10.1088/0959-5309/43/5/301.

[19] Simon Stephan, Martin T. Horsch, Jadran Vrabec & Hans Hasse. MolMod–an open access database of force fields for molecular simulations of fluids, *Molecular Simulation*, vol. 45, no. 10, pp. 806-814, 2019. Available: https://doi.org/10.1080/08927022.2019.1601191.

[20] N. Tchipev, S. Seckler, M. Heinen, J. Vrabec, F. Gratl, M. Horsch, M. Bernreuther, C. W. Glass, C. Niethammer, N. Hammer, B. Krischok, M. Resch, D. Kranzlmüller, H. Hasse, H.-J. Bungartz, and P. Neumann, "Twetris: Twenty trillion-atom simulation," *The International Journal of High Performance Computing* Applications, vol. 33, no. 5, pp. 838–854, 2019. Available: https://doi.org/10.1177/1094342018819741.

[21] Jones, J. E. "On the determination of molecular fields. —II. From the equation of state of a gas". *Proceedings of the Royal Society of London. Series A, Containing Papers of a Mathematical and Physical Character*, vol. 106 no. 738, pp. 463–477, 1924. Available: https://doi.org/10.1098/rspa.1924.0082.

[22] Wood, W. W.; Parker, F. R. "Monte Carlo Equation of State of Molecules Interacting with the Lennard-Jones Potential. I. A Supercritical Isotherm at about Twice the Critical Temperature". *The Journal of Chemical Physics*, vol. 27, no. 3, pp. 720–733, 1957. Available: https://doi.org/10.1063/1.1743822.

[23] S. Dubrovskiy and K. Gareev, "Measurement method for detecting magnetic and dielectric properties of composite materials at microwave frequencies", *2015 IEEE NW Russia Young Researchers in Electrical and Electronic Engineering Conference*, St. Petersburg, pp. 24-26, 2015. Available: https://doi.org/10.1109/EIConRusNW.2015.7102223.

[24] Grove, Timothy & Masters, Mark & Meirs, Richard. *Determining Dielectric Constants Using a Parallel Plate Capacitor*. Physics Faculty Publications, 2005. Available: https://doi.org/10.1119/1.1794757.

[25] Boltaev, A.P., Pudonin, F.A. & Sherstnev, I.A. "Low-frequency giant effective permittivity of island metal films", *Physics of the Solid State*, vol. 57, pp. 2099–2105, 2015. Available: https://doi.org/10.1134/S1063783415100066.

[26] Costa, F., Amabile, C., Monorchio, A., Prati, E. "Waveguide Dielectric Permittivity Measurement Technique Based on Resonant FSS Filters", *IEEE Microwave and Wireless Components Letters*. vol. 21, no. 5, pp. 273, 2011. Available: https://doi.org/10.1109/LMWC.2011.2122303.